CAMBRIDGE
UNIVERSITY PRESS

RESEARCH PAPER

Iron reduction as a viable metabolic pathway in Enceladus' ocean

Matthew J. Roche[1] (iD), Mark G. Fox-Powell[2], Rachael E. Hamp[2] and James M. Byrne[1]

[1]School of Earth Sciences, University of Bristol, Wills Memorial Building, Bristol BS8 1RJ, UK
[2]AstrobiologyOU, The Open University, Milton Keynes MK7 6AA, UK
Corresponding author: Matthew J. Roche; Email: matthew.roche@bristol.ac.uk

Abstract
Recent studies postulated the viability of a suite of metabolic pathways in Enceladus' ocean motivated by the detection of H_2 and CO_2 in the plumes – evidence for available free energy for methanogenesis driven by hydrothermal activity at the moon's seafloor. However, these have not yet been explored in detail. Here, a range of experiments were performed to investigate whether microbial iron reduction could be a viable metabolic pathway in the ocean by iron-reducing bacteria such as *Geobacter sulfurreducens*. This study has three main outcomes: (i) the successful reduction of a number of crystalline Fe(III)-bearing minerals predicted to be present at Enceladus was shown to take place to differing extents using acetate as an electron donor; (ii) substantial bacterial growth in a simulated Enceladus ocean medium was demonstrated using acetate and $H_{2(g)}$ separately as electron donors; (iii) microbial iron reduction of ferrihydrite was shown to partially occur at pH 9, the currently accepted value for Enceladus' ocean, whilst being severely hindered at the ambient ocean temperature of 0°. This study proposes the possibilities for biogeochemical iron cycling in Enceladus' ocean, suggesting that a strain of iron-reducing bacteria can effectively function under Enceladus-like conditions.

Contents

Introduction

Enceladus has become a prime target for astrobiological studies in recent years, owing to the discovery of a global subsurface ocean – a product of tidal heating (Thomas *et al.*, 2016; Choblet *et al.*, 2017) – and evidence for ongoing hydrothermal activity (Hsu *et al.*, 2015; Waite *et al.*, 2017). Current work has provided critical constraints on the ocean composition, temperature ($\sim 0°C$), seafloor pressure ($\sim 40 -$ 100 bar), pH (pH ~ 9) and salinity ($\sim 0.5 - 4\%$) (Postberg *et al.*, 2009, 2011; Hsu *et al.*, 2015; Glein *et al.*, 2018; Glein and Waite, 2020; Fox-Powell and Cousins, 2021), and on the nature of the proposed alkaline vent systems ($\geq 90°C$) at the moon's ocean floor (Hsu *et al.*, 2015; Sekine *et al.*, 2015). These constraints show that the conditions in Enceladus' ocean environment are well within the tolerable range of microorganisms and are comparable to conditions found at alkaline hydrothermal vents on Earth. This has motivated detailed work into further understanding the nature of Enceladus' seafloor and its potential habitability.

On Earth, the *Lost City* hydrothermal vent system located ~ 15 km off the mid-Atlantic ridge is a well-studied example of low temperature ($\leq 116°C$), alkaline (pH 9–11) hydrothermal activity (Kelley *et al.*, 2005). The vent chimneys ultimately are a result of serpentinization reactions that exothermically generate H_2- and CH_4-rich fluids (with traces of formate and acetate), with the vents themselves built by inorganic carbon precipitation as carbonates at high pH (Kelley *et al.*, 2005; Russell *et al.*, 2010). Analogous activity at Enceladus' seafloor has been postulated; the detection of salts in the plume material (Postberg *et al.*, 2009) served as crucial evidence for contact between the core and subsurface ocean. Later detection of silica nanoparticles in Saturn's E-ring (Hsu *et al.*, 2015) and $H_{2(g)}$ in the plumes (Waite *et al.*, 2017) indicated ongoing high-temperature hydrothermal reactions with a silicate interior dominated by serpentine group minerals. Additionally, estimates of the ocean pH and vent temperatures (Postberg *et al.*, 2009; Hsu *et al.*, 2015; Glein *et al.*, 2018; Glein and Waite, 2020) correspond well to measurements made at alkaline vents on Earth, adding further evidence that Enceladus' ocean floor is hydrothermally active.

Alkaline vent systems on Earth harbour diverse communities of microbial life, including chemotrophic methane-oxidizing and sulphur-oxidizing/-reducing bacteria, and methanogenic and anaerobic methane-oxidizing bacteria and archaea (Kelley *et al.*, 2005). Iron oxidizing bacteria have also been documented in alkaline hydrothermal regions analogous to the conditions expected at Enceladus (Scott *et al.*, 2015). The chemical gradients found at these vents have led to suggestions that these ocean environments are the prime candidates for observing prebiotic chemistry at play and possibly where life on Earth began (e.g. Russell *et al.*, 1989, 1994, 2010, 2014). The redox potential that could exist between Enceladus' reducing core/vent environments and the more oxidized ocean means that chemical energy should be in abundance and could in fact be exploited by microorganisms to drive their metabolism (McKay *et al.*, 2014; Barge and White, 2017; Deamer and Damer, 2017; Angelis *et al.*, 2021). Additionally, all six bioessential elements necessary to drive prebiotic chemistry and form biomass (carbon, hydrogen, nitrogen, oxygen, phosphorous and sulphur) have now been detected (or in the case of sulphur, tentatively detected) in the plumes by the *Cassini* spacecraft along with a suite of astrobiologically relevant organic phases (Waite *et al.*, 2006, 2009, 2017; Hansen *et al.*, 2011, 2020; Postberg *et al.*, 2018a, 2018b, 2023; Hao *et al.*, 2022). Of particular note is the recent confirmation of phosphorous at Enceladus, which was previously considered a biological limitation owing to its initial non-detection. The detection of sodium phosphate salts in the Cosmic Dust Analyser (CDA) data (Postberg *et al.*, 2023) and the results of geochemical models predict the concentrations of dissolved phosphorous to be similar to, or even higher, than in the Earth's oceans (Hao *et al.*, 2022).

The detection of H_2 and CO_2 in the plumes led to the suggestion that methanogenesis could be a possible, and energetically favourable, metabolic pathway for life at Enceladus (Waite *et al.*, 2017; Taubner *et al.*, 2018; Higgins *et al.*, 2021; Tenelanda-Osorio *et al.*, 2021). Affholder *et al.* (2021) even suggested that the CH_4 detected in the plumes is biogenic in origin. Ray *et al.* (2021) was the first study to explore the possibilities for other metabolic pathways, such as those involving iron or

sulphur, under Enceladus-like conditions, and to suggest that Enceladus' ocean could host a diverse ecosystem of microbial communities in competition for available resources. To date, no studies have attempted to experimentally culture cells using, for example, iron- or sulphur-bearing substrates as the electron donor/acceptor, or in a medium analogous to Enceladus' ocean composition. Studies which have cultured any microbe under Enceladus-relevant conditions (e.g. temperature, pH) are particularly rare. This study has paved the way for exploring, both experimentally and computationally, the possibility for other common terrestrial metabolisms under Enceladus-like conditions.

Microbial respiration of iron is the primary control on the mobility and reactivity of iron in the environment on Earth; iron can be biotically transformed between its soluble ferrous (Fe(II)) and insoluble ferric (Fe(III)) states via a variety of different reductive and oxidative pathways involving sunlight, nitrogen-, sulphur- and manganese-bearing species, organic carbon and H_2 (Weber *et al.*, 2006; Kappler *et al.*, 2021). These biotic reactions can occur simultaneously with abiotic reactions, leading to the development of a complex biogeochemical iron cycle (Kappler *et al.*, 2021). Furthermore, it is thought that life originated on a hot, Fe(II)-rich early Earth (e.g. Russell *et al.*, 1989, 1994), meaning that iron-based metabolisms were likely some of the first to evolve and are thus an ancient and primitive form of respiration (Weber *et al.*, 2006), which could be of importance to the development of life at Enceladus.

Whilst iron minerals have not yet been found in abundance around alkaline vent systems such as the *Lost City*, recent studies are showing that multivalent green rust minerals such as fougèrite should form naturally in these environments where they could play key roles in the development of primitive iron-based metabolisms (Russell, 2018; Trolard *et al.*, 2021). Amakinite, another green rust mineral, has previously been documented around alkaline vents on Earth (Beard *et al.*, 2009; Klein *et al.*, 2009; Boschi *et al.*, 2017) and in carbonaceous chondrites (Pignatelli *et al.*, 2016) – the proposed composition for Enceladus' core (Sekine *et al.*, 2015). CI and CM chondrites, two varieties of carbonaceous chondrite which have undergone significant aqueous alteration (Sephton, 2002), are likely most representative of Enceladus' interior given the evidence for ongoing water–rock interactions (Hsu *et al.*, 2015). Both are known to contain high, although differing, percentages of iron-bearing minerals including phyllosilicates (e.g. serpentine (such as cronstedtite), which could constitute 60–80% of the mineralogy; saponite), olivine (compositions between forsterite and fayalite), iron oxides (e.g. magnetite; ferrihydrite), pyroxene and sulphides (e.g. pyrrhotite; pentlandite) (Tomeoka and Buseck, 1985; Zolensky *et al.*, 1993; Endreß *et al.*, 1996; Rosenberg *et al.*, 2001; King *et al.*, 2015). Geochemical models of water–rock interactions at Enceladus performed by Hamp (2022), Ray *et al.* (2021) and Sekine *et al.* (2015) have also predicted the presence of a variety of other iron-bearing minerals at Enceladus which are summarized in Table 1. In addition, prior work has shown that Enceladus' ocean fluid also likely contains a variety of oxidized and reduced iron species, albeit at unconstrained concentrations (Zolotov, 2007; Sekine *et al.*, 2015; Glein and Waite, 2020; Hamp, 2022). Although the exact composition of Enceladus' core and whether its composition is best represented by either CI or CM chondrites is currently uncertain, it is highly likely that a variety of Fe(II)- and Fe(III)-bearing phases are present in Enceladus' core or are being formed by hydrothermal water–rock interactions.

Based on the prospect of Enceladus' core hosting a range of iron-bearing minerals, we have built upon the results of work of Ray *et al.* (2021) and Hamp (2022) and performed a range of geomicrobiological and geochemical laboratory experiments to investigate the viability of iron reduction and the possibilities for a biogeochemical iron cycle under Enceladus-like conditions. We identified three main questions which we aimed to address:

(a) *Given our current knowledge of the Fe(III)-bearing minerals that should be present in the chondritic core, can iron-reducing bacteria access the Fe(III) in these minerals for their metabolism?*

Fe(III)-bearing minerals, predicted to be present in Enceladus' chondritic core or at the seafloor vent environments by geochemical models performed by Ray *et al.* (2021) and Hamp (2022), were exposed to an anaerobic strain of iron-reducing bacteria at circumneutral pH, and the rate and extent of iron reduction monitored over time.

Table 1. *Iron-bearing minerals predicted to be present at Enceladus based on geochemical models and laboratory experiments*

Mineral	Formula
Celadonite[a]	$K(Mg,Fe^{2+})(Fe^{3+},Al)Si_4O_{10}(OH)_2$
Cronstedtite[b]	$\mathbf{Fe_2^{2+}Fe^{3+}(Si,Fe^{3+}O_5)(OH)_4}$
Greenalite[b]	$(Fe^{2+},Fe^{3+})_{2-3}Si_2O_5OH_4$
Haematite[a]	$\boldsymbol{\alpha}\text{–}\mathbf{Fe_2^{3+}O_3}$
Magnetite[a,b,c]	$\mathbf{Fe^{2+}Fe_2^{3+}O_4}$
Minnesotaite[b]	$(Fe^{2+},Mg)_3Si_4O_{10}(OH)_2$
Nontronite[a]	$(CaO_{0.5},Na)_{0.3}Fe_2^{3+}(Si,Al)_4O_{10}(OH)_2 \cdot n(H_2O)$
Olivine[c]	$(Mg,Fe^{2+})SiO_4$
Pyrite[a]	$Fe^{2+}S_2$
Pyroxene[c]	$XY(Si,Al)_2O_6$, where $X \stackrel{?}{=} Fe^{2+}$ & $Y \stackrel{?}{=} Fe^{2+}$ or Fe^{3+}
Saponite[c]	$Ca_{0.25}(Mg,Fe^{2+})_3((Si,Al)_4O_{10})(OH)_2 \cdot n(H_2O)$
Serpentine (Antigorite, Chrysotile)[a,b]	$(Mg,Fe^{2+})_3Si_2O_5(OH)_4$
Siderite[a]	$Fe^{2+}CO_3$

[a]Hamp (2022).
[b]Ray *et al.* (2021).
[c]Sekine *et al.* (2015).
Minerals in **bold** typeface are those that were used in this study.

(b) *Given our knowledge of the composition of Enceladus' ocean, can iron-reducing bacteria grow in a synthesized fluid analogous to the ocean's composition?*

A growth medium analogous to the composition of Enceladus' ocean, based on the work of Fox-Powell and Cousins (2021), was synthesized, inoculated with an anaerobic strain of iron-reducing bacteria, and the rate and extent of growth monitored over time.

(c) *Is microbial iron reduction possible under temperature and pH conditions relevant to Enceladus?*

The rate and extent of reduction of the poorly crystalline Fe(III)-oxyhydroxide mineral ferrihydrite, not yet thought to be present at Enceladus but here used due to its excellent ability to act as an electron sink, was monitored at pH 9 and 0°C – values considered relevant for Enceladus' ocean and its ambient temperature (Hsu *et al.*, 2015; Waite *et al.*, 2017; Glein and Waite, 2020).

This study demonstrates that iron-reducing bacteria can effectively function under Enceladus-like conditions, setting the stage for more detailed laboratory and computational work on biogeochemical iron cycling in Enceladus' ocean and the possible biosignatures that these metabolisms may produce.

Materials and methods

Summary

Three main experiments were performed to investigate the viability of microbial iron reduction in Enceladus' ocean.

(a) Firstly, the extents and rates of reduction of four Fe(III)-bearing minerals by a strain of iron-reducing bacteria were tested, using riboflavin as an electron shuttle. The minerals chosen were ferrihydrite (used as a positive control), magnetite, haematite and cronstedtite, and were selected based on the results of geochemical models of water–rock interactions in the Enceladus' alkaline hydrothermal environment by Hamp (2022) and Ray *et al.* (2021), but also on the availability of Enceladus-relevant Fe(III)-bearing minerals (see Table 1) during the short time frame that this study was performed. Ferrihydrite and magnetite were synthesized as the materials required for

their synthesis were readily available at the time, and synthesis helps us to control the purity of the end product. Similarly, the iron-reducing strain (*Geobacter sulfurreducens*, hereafter abbreviated to *G. sulfurreducens*) and electron shuttle used were selected as they were readily available for use in the biogeochemistry laboratory at the University of Bristol's School of Earth Science at the time the study was performed. Ideally, an alkaliphilic, halophilic strain more tolerant of the conditions expected at Enceladus would have been chosen, however these were not available. Ferrozine measurements were performed to measure the amounts of soluble Fe(II) being released into solution as microbial reduction took place, whilst magnetic susceptibility measurements were performed to probe whether the magnetic properties of the minerals were changing over the course of the reduction, which could inform us about possible mineral transformations. For example, magnetite is an expected product of the microbial reduction of ferrihydrite and thus we expect a clear increase in the magnetic susceptibility of the sample over the course of the experiment owing to magnetite's magnetic properties. The purity of the starting minerals was assessed using X-ray diffraction. Scanning electron microscopy was used to image the mineral samples before and after any reduction had taken place to search for any visible changes in mineral morphology.

(b) Secondly, the rate and extent of growth of *G. sulfurreducens* in a simulated Enceladus ocean medium adapted from Fox-Powell and Cousins (2021) (Table 3) was measured and compared to growth in a normal basal medium (Table 2). Both acetate and $H_{2(g)}$ were tested as electron donors as they are expected to be emitted by alkaline vents at Enceladus' seafloor and are known to be used as electron donors by terrestrial iron-metabolizing bacteria (Kelley *et al.*, 2005; Weber *et al.*, 2006; Russell *et al.*, 2010). The rate and extent of growth was tracked by measuring changes in the optical density of the solutions over time, such that a higher number of bacteria in solution corresponds to a more optically dense solution.

(c) Finally, the extents and rates of microbial iron reduction at pH 7 and 9, and at 0°C and 28°C, were monitored, using ferrihydrite as the sole mineral due to its excellent ability to act as an electron sink. Ferrozine and magnetic susceptibility measurements were performed based on the rationale described previously, with scanning electron microscopy similarly used for mineral characterization.

Preparation of starting materials

Mineral preparation

Ferrihydrite synthesis
Two-line ferrihydrite (general formula, $Fe_2^{3+}O_3 \cdot 0.5H_2O$) was synthesized according to the method detailed in Schwertmann and Cornell (2000). Forty grams of $Fe(NO_3)_3$ was dissolved in 500 ml Milli-Q H_2O before the addition of 310 ml KOH (1 M) solution whilst vigorously stirring. The pH was raised slowly to ~7.3 by adding an extra 20 ml KOH (1 M) dropwise, and the suspension let to sit for 2 h without stirring. The pH, which had now dropped to ~6, was then readjusted to a final pH of 7.5 with 1 M KOH. The suspension was transferred to centrifuge tubes and centrifuged at 4,000 g for 10 min, the supernatant discarded and the solid washed four times with 1 litre Milli-Q H_2O. The solid was then resuspended in Milli-Q H_2O and transferred to a serum vial.

Magnetite nanoparticle synthesis
Magnetite ($Fe^{2+}Fe_2^{3+}O_4$) nanoparticles (diameter ~12 nm) were synthesized according to the method detailed in Pearce *et al.* (2012). A total of 1.9881 g $FeCl_2 \cdot 4H_2O$ and 5.4059 g $FeCl_3 \cdot 6H_2O$ were weighed out into a volumetric flask and 60 ml HCl (0.3 M) was added. The solution was mixed well until all solids were dissolved, and the flask was topped up to 100 ml with extra 0.3 M HCl. A solution of 35% NH_4OH was diluted to 20% with Milli-Q H_2O, then sparged with N_2 for 20 min. The acidified Fe(II)/Fe(III) solution was added dropwise to 100 g of the 20% NH_4OH solution whilst vigorously stirring until all the solution had been added and a black precipitate had formed. The

Table 2. *Salt components of the basal medium for* G. sulfurreducens

Constituent	Mass concentration (g l^{-1} H_2O)
KH_2PO_4	0.6
NH_4Cl	0.3
$MgSO_4 \cdot 7H_2O$	0.5
$CaCl_2 \cdot 2H_2O$	0.1

Table 3. *Salt components of the Enceladus ocean simulant medium*

Constituent	Mass concentration (g l^{-1} H_2O)
NaCl	11.74
NH_4Cl	0.0542
$Na_2HPO_4 \cdot 2H_2O$	0.0630
KCl	0.172
$MgCl_2 \cdot 6H_2O$	0.0206
$CaCl_2 \cdot 2H_2O$	0.00298
$NaHCO_3$	2.52
Na_2SiO_3	0.412

solution was sealed in a Schott bottle, the headspace flushed with N_2 for 5 min and let to sit whilst stirring for 15 min. The solid precipitate was washed twice with anoxic Milli-Q H_2O in the glovebox and then sealed in a serum vial.

Haematite and cronstedtite preparation

A sample of haematite (α–$Fe_2^{3+}O_3$) was obtained from the University of Bristol School of Earth Sciences collection. A sample of cronstedtite ($Fe_2^{2+}Fe^{3+}(Si,Fe^{3+}O_5)(OH)_4$), listed to occur with hisingerite ($Fe_2^{3+}(Si_2O_5)(OH)_4$) and quartz, was sourced from National Museums Scotland. The samples were crushed with a rock hammer on a metal plate until the fragments were ~2 mm in size, and then milled for 10 min in a Retsch PM100 planetary ball mill until a fine powder (~1 µm) was achieved. Cronstedtite was milled using a 50 ml agate grinding jar, whilst haematite was milled using a much stronger and more efficient 250 ml SiN grinding jar.

Mineral characterization

Ferrozine assay

The Fe^{2+} and total iron content (hereafter denoted as Fe(II) and Fe_{tot}, respectively) of each mineral was assessed spectrophotometrically in triplicate using the ferrozine assay (Stookey, 1970; Viollier *et al.*, 2000). To measure dissolved Fe(II), 1 ml of sample was taken from each vial and centrifuged for 1 min at 14,500 g until a solid pellet separated from the solution. In total, 80 µl HCl (1 M) was added to each well in a 96-well plate along with 20 µl of sample (taken from the aqueous fraction of centrifuged sample) or standard ($(NH_4)_2Fe(SO_4)_2 \cdot 6H_2O$ in 1 M HCl, with Fe concentrations in the range of 0–1000 µM) and 100 µl ferrozine (Na_2-3-(2-pyridl)-5-6-bis(4-phenylsulfonate)-1,2,3-triazine). The plate was left to incubate in the dark for 5 min and the absorbance of each sample measured at λ = 562 nm in a Multiskan SkyHigh Microplate Spectrophotometer. To measure Fe_{tot}, 80 µl 10% w/v hydroxylamine hydrochloride (HAHCl) in 1 M HCl was added to each well along with 20 µl

sample or standard, and left to incubate in the dark for 30 min. In total, 100 µl ferrozine was added to each well and left to incubate in the dark for 5 min. The absorbance of each sample was then measured as above.

Magnetic susceptibility

The magnetic susceptibility of each mineral was measured at low frequency using a Bartington MS2B frequency-dependent magnetic susceptibility meter.

X-Ray diffraction (XRD)

X-ray diffraction (XRD) measurements were carried out on a Bruker D8 Advance diffractometer with a PSD LynxEye detector and Cu K$_\alpha$ radiation (1.540600 Å) to better assess the mineralogy of each sample. The samples were placed on a low background silicon wafer holder. XRD data were collected in the range of 5–75° 2θ with a step size of 0.02° 2θ, where the time per step was 1 s.

Basal medium and bacteria stock preparation

In a 1 litre Schott bottle, basic salts (Table 2) were dissolved in 950 ml Milli-Q H$_2$O, whilst NaHCO$_3$ was dissolved separately in 50 ml anoxic MilliQ H$_2$O. Both bottles were autoclaved to sterilize, then combined in the 1 litre bottle with a needle and syringe to achieve a NaHCO$_3$ concentration of 30 mM. The bottle headspace was then flushed with 80:20 N$_2$:CO$_2$ gas mixture for 10 min. A total of 1 ml litre^{-1} concentrations of trace elements SL10, 7 vitamins solution, and selenite/tungstate solution were added to the bottle along with 25 ml sodium acetate (CH$_3$COONa, denoted as acetate elsewhere) (1 M) and 40 ml sodium fumarate (C$_4$H$_2$Na$_2$O$_4$) (1 M), and the pH adjusted to ∼7 with anoxic 1 M HCl/0.5 M Na$_2$CO$_3$.

In total, 50 ml of medium was decanted into seven 100 ml serum vials; one vial was inoculated with 10% v/v *G. sulfurreducens* and then incubated at 28°C to promote growth. Five millilitres (10% v/v) solution was decanted from this vial into the six remaining bottles. After 2 days of growth, the optical density of the vials was measured using a Multiskan SkyHigh Microplate Spectrophotometer at $\lambda = 600$ nm. The contents of the six vials were added to sterile, anoxic centrifuge tubes, their masses equalized with sterile NaHCO$_3$ (30 mM), and centrifuged at 4,000 g for 20 min to separate the solid and liquid fractions. The supernatants were then discarded, and the solid fractions consolidated into one tube before washing another twice with sterile NaHCO$_3$ (30 mM). The contents of the final consolidated tube were added to a 30 ml serum vial, and the optical density of this concentrated stock measured to assess the volume of bacteria required to add to each serum vial.

Incubation experiments

Mineral reduction experiments

Under sterile conditions, 20 ml serum vials were prepared containing 0.2 ml sodium acetate (0.1 mM; concentration of 2 mM per vial) as the electron donor, iron minerals (see below) as the electron acceptor, 0.1 ml riboflavin (0.01 mM) as an electron shuttle, and buffered with NaHCO$_3$ (30 mM). Samples were prepared in triplicate such that for each mineral, three vials contained mineral + bacteria + electron shuttle, three contained mineral + bacteria, and the final three contained only mineral. The minerals haematite and cronstedtite were added to individual bottles as dried powders (0.0715 and 0.0228 g, respectively), whereas ferrihydrite and magnetite were added from liquid suspensions (0.16 ml from a 628 mmol l^{-1} stock and 0.27 ml from a 123 mmol l^{-1} stock, respectively). Each vial was sealed with a grey butyl stopper, manufactured by Supelco (product number 27232), and flushed with 80:20 N$_2$:CO$_2$ gas mixture for 1 min to achieve an anoxic headspace. Setups designed to be measured using magnetic susceptibility were crimped with rubber heat shrink tubing to avoid interference with the instrument, with all others crimped using standard aluminium caps. Setups containing bacteria

were inoculated with *G. sulfurreducens* (10% v/v) grown to the late lag phase at standard conditions. Ferrozine analysis and measurements of the samples' magnetic susceptibility were performed as described previously.

Bacterial growth experiments

In total, 100 ml serum vials were prepared with 50 ml of medium, inoculated with 10% v/v *G. sulfurreducens*, and incubated at 28°C to promote growth. Three different media were used: (i) normal growth medium (see *Basal medium and bacteria stock preparation*); (ii) an Enceladus ocean simulant medium; and (iii) a diluted Enceladus ocean simulant medium, each initially containing only 20 ml sodium fumarate (1 M). A total of 1.25 ml sodium acetate (1 M) and 80:20 H_2:CO_2 gas mixture were added separately to act as electron donors; for those containing H_2/CO_2, the headspace of each bottle was flushed initially for 5 min before inoculation, then flushed for 1 min after sampling.

The Enceladus ocean simulant medium was adapted from Fox-Powell and Cousins ([2021](#)). In a 500 ml Schott bottle, salts ([Table 3](#)) were dissolved in 400 ml MilliQ H_2O, except $NaHCO_3$ and Na_2SiO_3 which were dissolved separately in 50 ml anoxic MilliQ H_2O in two more Schott bottles. All three bottles were then autoclaved to sterilize, and the 50 ml solutions of $NaHCO_3$ and Na_2SiO_3 added to the 400 ml salt solution with a needle and syringe. In a second 500 ml Schott bottle, 50 ml of the Enceladus ocean simulant was added to 450 ml anoxic $NaHCO_3$ (30 mM) solution to produce a 10× diluted ocean simulant with an ionic strength similar to that of the normal basal medium prepared in *Basal medium and bacteria stock preparation*; the solution was then autoclaved to sterilize. The headspace of both the concentrated and dilute Enceladus ocean simulants was flushed with 80:20 N_2:CO_2 gas mixture for 10 min, and then 1 $ml \, l^{-1}$ concentrations of trace elements SL10 and seven vitamins solution were added to each along with 20 ml sodium fumarate (1 M). The pH of both solutions was adjusted to ~7 with anoxic 1 M HCl/0.5 M Na_2CO_3, before decanting into serum vials.

Environmental simulation experiments

Samples were prepared in triplicate such that for each condition (pH 7/28°C, pH 9/28°C and pH 7/0°C), three vials contained ferrihydrite + bacteria and three contained only ferrihydrite. Under sterile conditions, two anoxic stock solutions containing $NaHCO_3$ (30 mM), sodium acetate (2 mM) and ferrihydrite (10 $mmol \, l^{-1}$) were synthesized and their pH values adjusted to ~7 and ~9, respectively, with anoxic 1 M HCl/0.5 M Na_2CO_3. Ten millilitre serum vials were then prepared containing 5 ml of this solution. Each vial was sealed with a grey butyl stopper, manufactured by Supelco (product number 27232), and flushed with 80:20 N_2:CO_2 gas mixture for 1 min to achieve an anoxic headspace. Setups designed to be measured using magnetic susceptibility were crimped with rubber heat shrink tubing to avoid interference with the instrument, with all others crimped using standard aluminium caps. Setups containing bacteria were inoculated with *G. sulfurreducens* (10% v/v). Half the number of vials containing pH 7 solution were placed into an incubator at 28°C whilst the other half were incubated at 0°C. The vials containing pH 9 solution were also incubated at 28°C. Ferrozine analysis and measurements of the samples' magnetic susceptibility were performed as described previously.

Characterization of end products

Scanning electron microscopy (SEM)

A total of 0.1 ml sample containing minerals ± bacteria were added to eppendorfs containing 0.9 ml $NaHCO_3$ (30 mM). In total, 25 µl of this was then pipetted onto glass slides and left to air dry, before sputter coating with carbon (~15 nm thick). Slides were mounted onto an aluminium stub and imaged at a working distance of ~15 mm using a Hitachi S-3500N at 20 kV. Both secondary electron (SE) and backscattered electron (BSE) images were taken.

Results

Mineral reduction experiments

The rates and extents of reduction of the crystalline Fe(III)-bearing minerals magnetite, haematite and cronstedtite – each predicted to be present in Enceladus' core material or formed through water–rock interactions (Ray *et al.*, 2021; Hamp, 2022) – by the iron-reducing strain *G. sulfurreducens* were tested at pH 7 with and without riboflavin as an electron shuttle. Ferrihydrite, a poorly crystalline mineral not thought to be present at Enceladus, was also tested and was used purely as a positive control. XRD spectra of haematite and cronstedtite are shown in Fig. S1. An XRD pattern could not be obtained for ferrihydrite as it is X-ray amorphous. Changes in the dissolved Fe(II) and magnetic properties over time for each mineral were measured, with the results reported in Figs. 1 and 2, respectively, and SEM images of select microcosm experiments are displayed in Fig. S2. Since changes in only the dissolved Fe(II) were measured, we expect the rates and extents of reduction reported here to be lower limits of the true values since adsorption of Fe(II) to the solid phase surfaces has not been accounted for.

Ferrihydrite (Fig. 1(a)) was rapidly reduced by the bacteria in just a few days, releasing around 1 mM Fe(II) into solution and forming a black magnetic precipitate, whilst the samples containing riboflavin were reduced in around 1 day, releasing over 1.5 mM Fe(II) into solution. The change in magnetic susceptibility (Fig. 2(a)) of the samples exposed to bacteria lags slightly behind the initial rapid rise in dissolved Fe(II) (Fig. 1(a)), but within a few days the mineral shows a dramatic change in its magnetic properties. The samples containing riboflavin become strongly magnetic within 1 week and peak at around 10 days ($\sim 17 \times 10^{-4}$ SI), whilst those containing just bacteria peak at around 2 weeks ($\sim 4.68 \times 10^{-4}$ SI) and show a more subtle increase in susceptibility. After around 10 days, both dissolved Fe(II) and magnetic susceptibility showed few further changes. In contrast, magnetite (Fig. 1(b)) was reduced far less readily with very little Fe(II) released into solution (≤ 0.21 mM), taking nearly 2 weeks to show any changes; the samples containing riboflavin were less readily reduced than those without, however. No changes in the magnetic susceptibility were observed (Fig. 2(b)). Haematite (Fig. 1(c)) steadily released up to ~ 0.73 and ~ 0.42 mM Fe(II) for samples with and without riboflavin, respectively, over the 23-day course of the experiment. Similarly to magnetite, no changes in the magnetic susceptibility were observed (Fig. 2(c)). SEM images (Figs. S2(a) and S2(b)) reveal highly crystalline mineral grains with blocky morphologies, and finer amorphous material dispersed between the crystals. Cronstedtite (Fig. 1(d)) was readily reduced and reached its peak in under 5 days, releasing up to ~ 0.67 and ~ 0.39 mM Fe(II) for samples with and without riboflavin, respectively. The dissolved Fe(II) quickly decreased to a minimum before settling and showing few further changes after around 10 days. The control sample containing neither bacteria nor riboflavin released ~ 0.66 mM Fe(II) into solution after around 10 days. The magnetic susceptibility of cronstedtite was not measured since no magnetic material was expected to be produced and no changes in the magnetic properties of this clay mineral were expected to be observed. SEM micrographs (Figs. S2(c) and S2(d)) show some differences between the control and end product of microbial reduction; the control mineral appears as an aggregate of fine blocky crystals whilst the cronstedtite exposed to bacteria instead appears as one large flattened crystal. Both show finer amorphous material dispersed between the larger crystals.

Bacterial growth experiments

The rate and extent of growth of *G. sulfurreducens* in a simulated Enceladus ocean medium (Figs. 3(b) and 3(c)) was measured and compared to growth in a normal basal medium (Fig. 3(a)), using both acetate and H$_2$ as electron donors and sodium fumarate as an electron acceptor. Within 1 week, the bacteria cultured in the normal basal medium (Fig. 3(a)) with acetate grew, turning the growth medium pink. Most growth occurred between days 4–7. The medium containing H$_{2\ (g)}$ also sustained growth but to a much lesser extent, with much of the growth occurring early on up to day 4. The bacteria cultured in the Enceladus ocean simulant medium (Fig. 3(b)) with acetate successfully sustained growth,
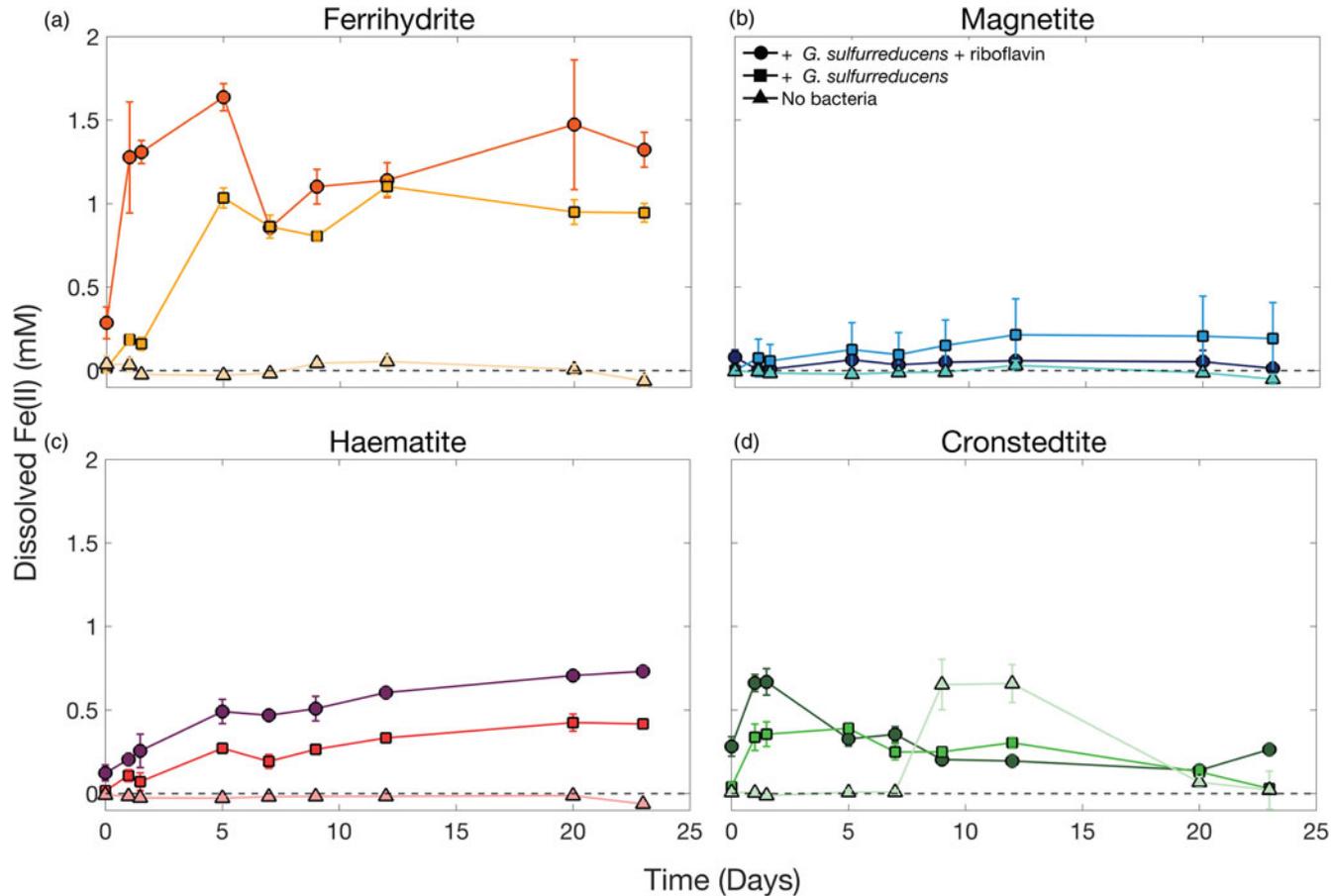
Figure 1. *Observed changes in dissolved Fe(II) over time from four different Fe(III)-bearing minerals at neutral pH (pH 7), with and without the presence of iron-reducing bacteria and riboflavin as an electron shuttle. Figures (a-d) represent the minerals ferrihydrite, magnetite, haematite and cronstedtite, respectively. Error bars indicate standard deviation from the mean.*
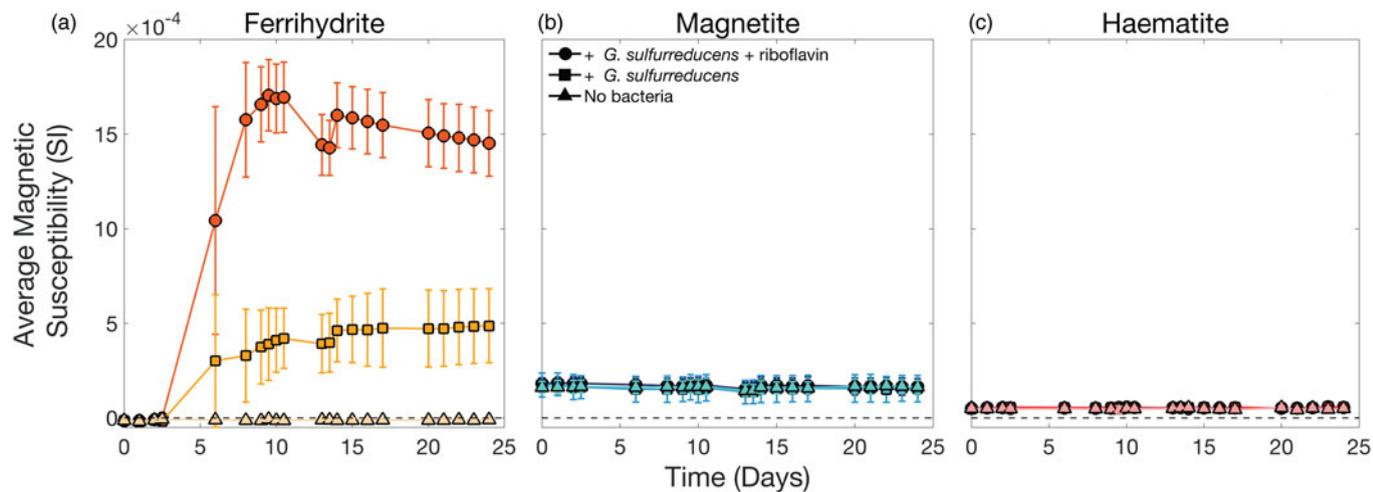
Figure 2. *Observed changes in the magnetic susceptibility over time of three different Fe(III)-bearing minerals at neutral pH (pH 7), with and without the presence of iron-reducing bacteria and riboflavin as an electron shuttle. Figures (a–c) represent the minerals ferrihydrite, magnetite and haematite, respectively. Error bars indicate the standard deviation from the mean.*
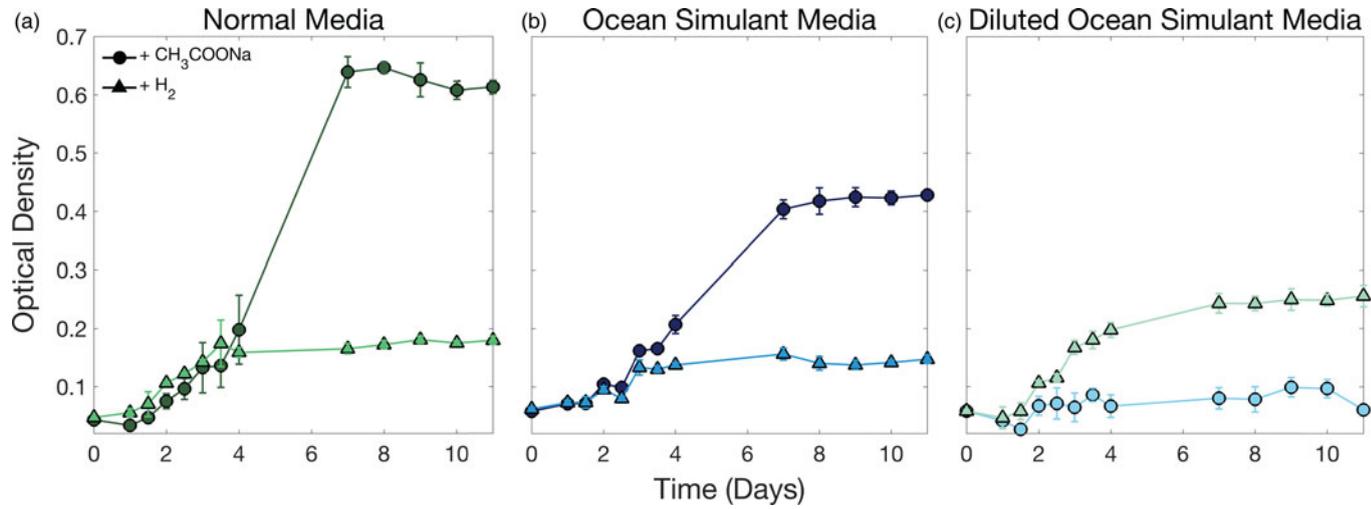
Figure 3. *Observed changes in the optical density over time of three different solutions inoculated with bacteria: normal basal medium (a), an Enceladus ocean simulant (b) and a diluted ocean simulant (c). Error bars indicate the standard deviation from the mean.*

comparable to growth levels seen in the normal basal medium. The medium containing H_2 showed comparable rates and extents of growth as in the normal basal medium. In contrast, the diluted ocean simulant medium (Fig. 3(c)) sustained better growth with H_2 as an electron donor rather than acetate, however less growth was generally observed than in the non-diluted ocean simulant medium.

Environmental simulation experiments

Here, the extents and rates of microbial reduction of ferrihydrite at non-standard Enceladus-relevant pH and temperature were compared to reduction under standard conditions. No riboflavin was used. Changes in dissolved Fe(II) were measured, with results reported in (Fig. 4). As mentioned previously, since changes to the solid phases were not measured, we expect the rates and extents of reduction reported here to be lower limits of the true values. Magnetic susceptibility data are reported in Fig. S3. Under standard conditions (pH 7 and 28°C, Fig. 4(a)), the ferrihydrite was rapidly reduced with much of the reduction taking place in the first 5 days, releasing a maximum of ∼1.13 mM Fe (II) into solution. The reduction rate then decreased with the dissolved Fe(II) showing few further changes after around day 10. A small amount of reduction was observed at pH 9 (Fig. 4(b)) in the presence of bacteria, with a maximum of only ∼0.07 mM Fe(II) released into solution by day 7. Almost no changes in the dissolved Fe(II) without bacteria were recorded. Little to no reduction was observed at 0°C (Fig. 4(c)), however, with a maximum of only ∼0.01 mM Fe(II) released into solution by the end of day 3.

Discussion

Structural effect of minerals on microbial iron reduction

In contrast to ferrihydrite, the bacteria reduced magnetite, haematite and cronstedtite much less readily likely due to their higher crystallinities and lower specific surface areas (it is unclear whether the finer amorphous material observed in the SEM images dispersed between the larger crystals are products of microbial iron reduction). This was unsurprising given that the difficulty for bacteria to reduce crystalline Fe(III)-bearing phases in the terrestrial environment has previously been documented (e.g. Weber *et al.*, 2006; Cutting *et al.*, 2009) and is thought to be due to the lower number of bioavailable active surface sites compared to amorphous phases. The SEM images of haematite support this, with its blocky morphology and highly crystalline nature likely hindering its susceptibility to microbial iron reduction.

The presence of riboflavin as an electron shuttle did enhance the extent of reduction in both haematite and cronstedtite, except for magnetite where the amount of reduction observed without riboflavin was greater. It is possible that the magnetite was already substantially reduced and thus oversaturated in electrons, meaning that reduction in the presence of riboflavin would have a lesser effect than without. Both haematite and cronstedtite show good potential for microbial iron reduction but over much longer timescales than ferrihydrite, suggesting that crystallinity may not be the sole control over the reduction potential. It is important to note, however, that the bacteria were grown using fumarate as an electron acceptor (see *Basal medium and bacteria stock preparation*) rather than an iron-bearing mineral. This ensured that there was no contamination of the iron minerals used here with any other sources of iron which could have been transferred across if pre-incubations were performed using an iron-bearing mineral rather than fumarate. However, this does mean that the bacteria would not be adapted (at least at the outset of the experiment) to using any of these minerals as electron acceptors. Therefore, we would expect somewhat reduced rates and extents of reduction.

Despite the lack of significant microbial iron reduction observed in these three minerals compared to ferrihydrite, the reduction of crystalline Fe(III)-bearing phases by alternative strains to *G. sulfurreducens* has been reported, specifically by the metal-reducing bacteria *Shewanella oneidensis* (Brookshaw *et al.*, 2014), *Shewanella putrefaciens* (e.g. Kostka and Nealson, 1995; Kostka *et al.*, 1996) and a variety of iron-reducing methanogens (Archaea) such as *Methanosarcina barkeri* (Liu *et al.*, 2011) and
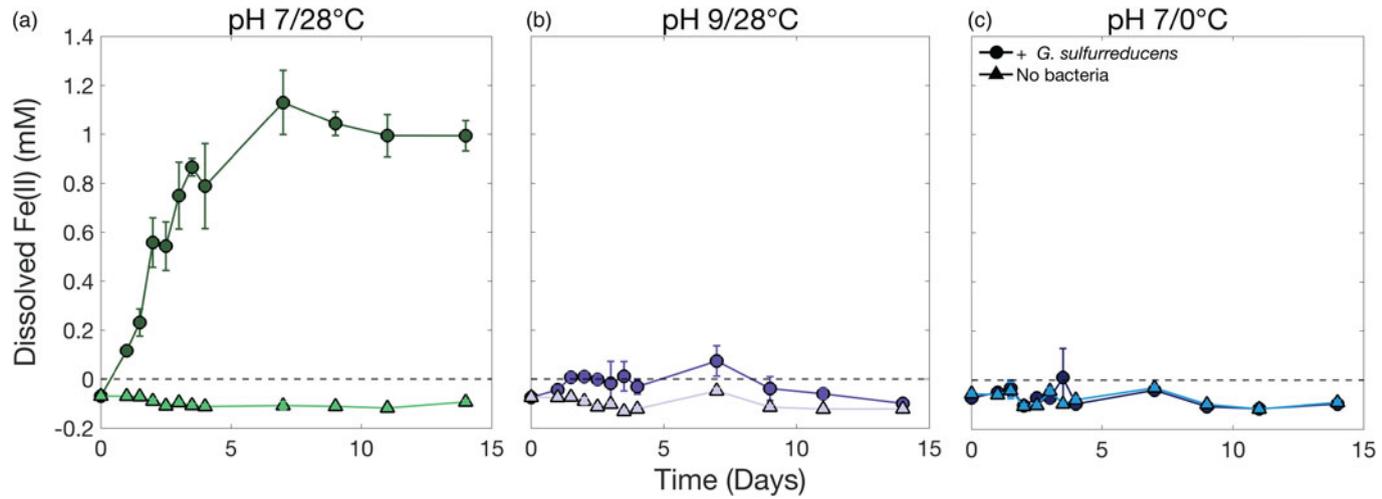
Figure 4. *Observed changes in dissolved Fe(II) derived from ferrihydrite over time at standard conditions (pH 7, 28°C) (a) and non-standard conditions, i.e. pH 9/28°C (b) and pH 7/0°C (c), with and without the presence of iron-reducing bacteria. Error bars indicate the standard deviation from the mean.*

Methanosarcina mazei (Zhang *et al.*, 2012). Oxidation of crystalline Fe(II)-bearing phases has also been reported using the photoferrotroph *Rhodopseudomonas palustris* (Byrne *et al.*, 2015, 2016). These studies have documented the reduction of phases including magnetite and the phyllosilicate minerals biotite and chlorite, but more importantly the hydrous aluminium-rich phyllosilicate clay minerals (smectite group) including nontronite – a mineral already predicted to be present at Enceladus (Hamp, 2022). It is possible that the layered structure of the clay mineral groups allow the bacteria to more readily access structural iron, especially in the presence of an electron shuttle. Cronstedtite is also a hydrous phyllosilicate mineral in the serpentine group, and in this study is shown to be readily reduced by *G. sulfurreducens* with and without the presence of an electron shuttle, thereby supporting this hypothesis. It is currently unclear, however, whether any compounds currently known in Enceladus' ocean could function as electron shuttles for microbial metabolisms. On Earth, redox-active organic molecules such as quinone- and hydroquinone-containing molecules present in natural organic matter most readily serve as electron shuttles in the environment (Bai *et al.*, 2020a, 2020c). Bai *et al.* (2020b) also show that high pH conditions can in fact promote the degradation of organic matter and thus the release of redox-sensitive aromatic compounds which could serve as electron shuttle for microbial iron reduction, meaning that the high pH of Enceladus' ocean could encourage the formation of these compounds. Whilst macromolecular organics have been detected in Enceladus' plumes (Postberg *et al.*, 2018b), it is uncertain whether quinones/hydroquinones are amongst them. This work has highlighted the importance of electron shuttles in the metabolism of crystalline minerals, thus identifying whether any of the organics detected in Enceladus' plumes could act as electron shuttles could be key to understanding whether any minerals present at Enceladus could be metabolized by bacteria in the ocean.

Additionally, cronstedtite here has shown the potential for natural release of Fe(II) into solution which, whilst unimportant for iron-reducing bacteria, could be utilized by iron-oxidizing bacteria. SEM images show that the cronstedtite exposed to bacteria appears largely unaffected whilst the cronstedtite control possibly appears to have naturally disaggregated and reformed as a clump of finer blocky material. Therefore, although the highly crystalline Fe(III)-bearing phases present in Enceladus' silicate core (e.g. magnetite) may not be readily accessed by iron-reducing bacteria, the products of water–rock interactions in the alkaline hydrothermal environment including haematite and cronstedtite (plus others not tested in this study such as clays including nontronite and green rust minerals) show much more promise, even with a strain not optimized for the reduction of crystalline materials. Furthermore, it is possible that the mineral assemblages and organic products (e.g. exopolysaccharides) produced during microbial transformation of such minerals could serve as biomarkers for microbial iron reduction, and could even be detected remotely by future spacecraft (Kashyap *et al.*, 2022).

Electron donor effect on bacterial growth

H_2 is generally less effective than acetate as an electron donor in both the normal basal medium and the Enceladus ocean simulant medium, with much less significant growth observed despite a comparable initial growth rate. Acetate directly dissolved in the media is much more readily bioavailable than gaseous H_2 which will need to undergo exchange and dissolution with the media itself before it can become bioavailable. Additionally, since the bacteria were pre-grown using acetate they will be well-adapted to using this as the electron donor; switching the available electron donor to H_2 requires time and energy for the bacteria to adapt. Microbial communities at Enceladus likely would not experience this problem however. The hydrothermal vent systems should provide a continuous supply of dissolved H_2, directly detected in Enceladus' plumes as $H_{2(g)}$ (Waite *et al.*, 2017), and acetate ions (CH_3COO^-), present at analogous alkaline vents on Earth (Kelley *et al.*, 2005; Russell *et al.*, 2010) and in carbonaceous chondrites (e.g. Cronin and Chang, 1993) (the proposed composition of Enceladus' core), into the ocean, meaning there should be multiple bioavailable species in the environment to serve as an electron donor for microbial iron reduction. Cultures in the diluted ocean simulant medium grew more successfully using H_2 as an electron donor. This may be due to a lessened efficiency of the

acetate-metabolizing mechanisms when the concentrations of essential elements and nutrients are diluted, however it is likely because there is simply more energy to be gained from the oxidation of H_2 than acetate. Despite the high salinity and ionic strength six times greater than the normal basal medium, the Enceladus ocean simulant medium shows excellent promise to sustain healthy cultures of bacteria, even a strain not optimized for saline conditions. Assuming that the ocean simulant medium is a good approximation for that of Enceladus' ocean based on the most recent sampling and model data, the ocean should contain all of the necessary ingredients at optimal concentrations to sustain communities of iron-reducing bacteria.

Although not investigated in this study, a number of species thought to be present in Enceladus' ocean could serve as viable oxidants for iron oxidizing bacteria. These include NO_3^-, O_2, and H_2O_2. Therefore, as a variety of both oxidizing and reducing agents are likely dissolved in the ocean (Ray *et al.*, 2021), it is possible that a whole biogeochemical iron cycle could be taking place.

Effect of pH and temperature on ocean habitability

Both alkaline pH and low temperatures affected the efficiency of microbial iron reduction. This is unsurprising since it has previously been documented that iron reduction becomes less energetically favourable at high pH (e.g. Marquart *et al.*, 2019), and that lower temperatures kinetically affect the rates of reduction. Microbial communities would therefore be expected to inhabit the warmer vent environments at Enceladus rather than live planktonically in the cold ocean, as is common around vent systems on Earth. Since *G. sulfurreducens* is a neutrophilic strain, most previous studies have involved neutral pH conditions. Few studies have tested the strain's capabilities at non-standard pH, especially high pH. Babauta *et al.* (2012), albeit studying how *G. sulfurreducens* behaves at acidic pH, performed experiments at pH as low as 6, noting that growth was completely inhibited below pH ∼5.5. Microbial iron reduction does not appear to be completely inhibited at alkaline pH, with the experiments conducted in this study showing a clear difference between those inoculated with bacteria and those without (the negative concentrations were likely achieved due to poor instrument sensitivity at low iron concentrations, but the relative trends can still be assessed). Microbial iron reduction has therefore been demonstrated at non-standard conditions with a suboptimal strain of bacteria; a strain optimized for alkaline conditions and tolerant of a wider temperature range would likely thrive in these conditions. As mentioned previously however, since the bacteria were grown using fumarate rather than an iron-bearing mineral as the electron acceptor, the bacteria would not initially be adapted to using ferrihydrite as an electron acceptor. Therefore, we would expect somewhat reduced rates and extents of reduction.

It seems plausible that Enceladus' ocean has the necessary ingredients and environmental conditions to be favourable for sustaining life, and in our case, iron-reducing bacteria. Life around hydrothermal vent systems on Earth, including the *Lost City*, often consists of many different coexisting species (Kelley *et al.*, 2005). A similar scenario could therefore be expected at Enceladus, meaning it is important to understand how different microbial species interact to understand the bigger picture of Enceladus' ocean habitability. Marquart *et al.* (2019), although focussing on biogeochemical cycling in terrestrial environments, present findings relevant to understanding how exactly iron reducers may interact with other microbial species at Enceladus – specifically, methanogens. Recent work has in fact shown that Enceladus' ocean environment should be both chemically and thermodynamically favourable for methanogens (Taubner *et al.*, 2018; Affholder *et al.*, 2021; Higgins *et al.*, 2021; Ray *et al.*, 2021; Tenelanda-Osorio *et al.*, 2021). Marquart *et al.* (2019) find that the proportions of methanogenesis and iron reduction taking place in a system is highly sensitive to pH with methanogenesis completely displacing iron reduction as the energetically favourable metabolism at alkaline pH where goethite was used as the iron source. Additionally, the efficiency of and balance between methanogenesis and iron reduction at alkaline pH where clay minerals were used as the iron source was much less affected, since the reduction of clay minerals includes fewer protons and thus is less sensitive to pH.

Whilst Ray *et al.* (2021) predict a much lower free energy availability for iron reduction in Enceladus' ocean, the results of Marquart *et al.* (2019) suggest that not only could methanogens and iron reducers

become increasingly syntrophic (i.e. increasingly dependent on one another for growth) at alkaline pH, the efficiency of these metabolisms should not be sensitive to pH when clay minerals serve as the iron source. Enceladus' ocean could possibly harbour communities of both methanogens and iron reducers feeding off iron-rich clay minerals. If more crystalline Fe(III)-bearing minerals served as the primary source, methanogenesis would likely completely outcompete and displace iron reduction as a viable metabolism. Sulphate reduction – another common terrestrial metabolism – is, however, known to be less sensitive to pH, often more favourable than iron reduction at alkaline pH (Postma and Jakobsen, 1996; Bethke *et al.*, 2011), and more energetically favourable than iron reduction under Enceladus-like conditions (Ray *et al.*, 2021). Additionally, communities of sulphate-reducing bacteria have already been discovered in a strong syntrophic relation with methanogens at the *Lost City* alkaline vent system (Kelley *et al.*, 2005; Brazelton *et al.*, 2006). However, the presence, concentration and distribution of sulphur-bearing species at Enceladus is largely unconstrained at present, meaning that it is uncertain how sulphate- and iron-reducing bacteria could behave together under Enceladus-like conditions. The complex and intimate relationship between these key metabolic pathways is yet to be explored to its full extent and contextualized for Enceladus' ocean–vent environment meaning that these suggestions are pure speculation. However, they would be interesting avenues for future work.

Conclusion

The recent work of Ray *et al.* (2021) postulated that Enceladus' ocean could play host to a metabolically diverse ecosystem of microbial life, paving the way for subsequent work to understand the viability of non-methanogenic metabolisms in the ocean–vent environment. This study has shown that not only is microbial iron reduction of crystalline Fe(III)-bearing phases formed during hydrothermal water–rock interactions possible, and at alkaline pH, but an iron-reducing strain can successfully grow in a simulated Enceladus ocean fluid using acetate and dissolved H_2 separately as electron donors – two vent-derived molecules that should in abundance in the ocean. This work has also highlighted the importance of electron shuttles in the metabolism of crystalline minerals, something which future studies should aim to better understand in the context of Enceladus. Impressively, this has been proven using a suboptimal strain of iron-reducing bacteria – one which is not well adapted to alkaline and saline conditions, to a wide range of temperatures, or to reducing highly crystalline minerals; future work would look to isolate an alkaliphilic, halophilic iron-reducing strain which would be much more tolerant of the conditions found in Enceladus' ocean. Furthermore, this work has added additional support for Enceladus as an astrobiological target in future missions, missions which could aim to detect iron in Enceladus' plumes or chemical signatures of biogeochemical iron cycling.

References

Affholder A, Guyot F, Sauterey B, Ferrière R and Mazevet S (2021) Bayesian analysis of Enceladus' plume data to assess methanogenesis. *Nature Astronomy* **5**, 1–10.

Angelis G, Kordopati GG, Zingkou E, Karioti A, Sotiropoulou G and Pampalakis G (2021) Plausible emergence of biochemistry in Enceladus based on chemobrionics. *Chemistry* **27**, 600–604.

Babauta JT, Nguyen HD, Harrington TD, Renslow R and Beyenal H (2012) pH, redox potential and local biofilm potential micro-environments within *Geobacter sulfurreducens* biofilms and their roles in electron transfer. *Biotechnology and Bioengineering* **109**, 2651–2662.

Bai Y, Mellage A, Cirpka OA, Sun T, Angenent LT, Haderlein SB and Kappler A (2020a) AQDS and redox-active NOM enables microbial Fe(III)-mineral reduction at cm-scales. *Environmental Science and Technology* **54**, 4131–4139.

Bai Y, Subdiaga E, Haderlein SB, Knicker H and Kappler A (2020b) High-pH and anoxic conditions during soil organic matter extraction increases its electron-exchange capacity and ability to stimulate microbial Fe(III) reduction by electron shuttling. *Biogeosciences* **17**, 683–698.

Bai Y, Sun T, Angenent LT, Haderlein SB and Kappler A (2020c) Electron hopping enables rapid electron transfer between quinone-/hydroquinone-containing organic molecules in microbial iron (III) mineral reduction. *Environmental Science and Technology* **54**, 10646–10653.

Barge LM and White LM (2017) Experimentally testing hydrothermal vent origin of life on Enceladus and other icy/ocean worlds. *Astrobiology* **17**, 820–833.

Beard JS, Frost BR, Fryer P, McCaig A, Searle R, Ildefonse B, Zinin P and Sharma SK (2009) Onset and progression of serpentinization and magnetite formation in olivine-rich troctolite from IODP Hole U1309D. *Journal of Petrology* **50**, 387–403.

Bethke CM, Sanford RA, Kirk MF, Jin Q and Flynn TM (2011) The thermodynamic ladder in geomicrobiology. *American Journal of Science* **311**, 183–210.

Boschi C, Dini A, Baneschi I, Bedini F, Perchiazzi N and Cavallo A (2017) Brucite-driven CO_2 uptake in serpentinized dunites (Ligurian Ophiolites, Montecastelli, Tuscany). *Lithos* **288**, 264–281.

Brazelton WJ, Schrenk MO, Kelley DS and Baross JA (2006) Methane- and sulfur-metabolizing microbial communities dominate the Lost City hydrothermal field ecosystem. *Applied and Environmental Microbiology* **72**, 6257–6270.

Brookshaw DR, Lloyd JR, Vaughan DJ and Pattrick RA (2014) Bioreduction of biotite and chlorite by a Shewanella species. *American Mineralogist* **99**, 1746–1754.

Byrne JM, Klueglein N, Pearce C, Rosso KM, Appel E and Kappler A (2015) Redox cycling of Fe (II) and Fe (III) in magnetite by Fe-metabolizing bacteria. *Science* **347**, 1473–1476.

Byrne JM, Van Der Laan G, Figueroa AI, Qafoku O, Wang C, Pearce CI, Jackson M, Feinberg J, Rosso KM and Kappler A (2016) Size dependent microbial oxidation and reduction of magnetite nano-and micro-particles. *Scientific Reports* **6**, 1–13.

Choblet G, Tobie G, Sotin C, Běhounková M, Čadek O, Postberg F and Souček O (2017) Powering prolonged hydrothermal activity inside Enceladus. *Nature Astronomy* **1**, 841–847.

Cronin JR and Chang S. (1993) Organic matter in meteorites: molecular and isotopic analyses of the Murchison meteorite. In Greenberg JM, Mendoza-Gómez CX and Pirronello V (eds). *The Chemistry of Life's Origins*, NATO ASI Series, vol. 416. Dordrecht: Springer, pp. 209–258.

Cutting R, Coker V, Fellowes J, Lloyd J and Vaughan D (2009) Mineralogical and morphological constraints on the reduction of Fe(III) minerals by *Geobacter sulfurreducens*. *Geochimica et Cosmochimica Acta* **73**, 4004–4022.

Deamer D and Damer B (2017) Can life begin on Enceladus? A perspective from hydrothermal chemistry. *Astrobiology* **17**, 834–839.

Endreß M, Zinner E and Bischoff A (1996) Early aqueous activity on primitive meteorite parent bodies. *Nature* **379**, 701–703.

Fox-Powell MG and Cousins CR (2021) Partitioning of crystalline and amorphous phases during freezing of simulated Enceladus ocean fluids. *Journal of Geophysical Research: Planets* **126**, e2020JE006628.

Glein CR and Waite JH (2020) The carbonate geochemistry of Enceladus' ocean. *Geophysical Research Letters* **47**, e2019GL085885.

Glein C, Postberg F and Vance S (2018) The geochemistry of Enceladus: composition and controls. In Schenk PM, Clark RN, Howett CJA, Verbiscer AJ and Waite JH (eds), *Enceladus and the Icy Moons of Saturn*, vol. 475. Tucson: University of Arizona Press, pp. 39–56.

Hamp RE (2022) *Geochemical cycling in the subsurface environment of Enceladus*. PhD Thesis.

Hansen CJ, Shemansky DE, Esposito LW, Stewart AIF, Lewis BR, Colwell JE, Hendrix AR, West RA, Waite Jr JH, Teolis B and Magee BA (2011) The composition and structure of the Enceladus plume. *Geophysical Research Letters* **38**, L11202.

Hansen CJ, Esposito LW, Colwell JE, Hendrix AR, Portyankina G, Stewart AI and West RA (2020) The composition and structure of Enceladus' plume from the complete set of Cassini UVIS occultation observations. *Icarus* **344**, 113461.

Hao J, Glein CR, Huang F, Yee N, Catling DC, Postberg F, Hillier JK and Hazen RM (2022) Abundant phosphorus expected for possible life in Enceladus's ocean. *Proceedings of the National Academy of Sciences* **119**, e2201388119.

Higgins PM, Glein CR and Cockell CS (2021) Instantaneous habitable windows in the parameter space of Enceladus' ocean. *Journal of Geophysical Research: Planets* **126**, e2021JE006951.

Hsu H-W, Postberg F, Sekine Y, Shibuya T, Kempf S, Horányi M, Juhász A, Altobelli N, Suzuki K, Masaki Y, Kuwatani T, Tachibana S, Sirono S, Moragas-Klostermeyer G and Srama R (2015) Ongoing hydrothermal activities within Enceladus. *Nature* **519**, 207–210.

Kappler A, Bryce C, Mansor M, Lueder U, Byrne JM and Swanner ED (2021) An evolving view on biogeochemical cycling of iron. *Nature Reviews Microbiology* **19**, 360–374.

Kashyap S, Sklute EC, Wang P, Tague Jr TJ, Dyar MD and Holden JF (2022) Spectral detection of nanophase iron minerals produced by Fe(III)-reducing hyperthermophilic Crenarchaea. *Astrobiology* **23**, 43–59.

Kelley DS, Karson JA, Früh-Green GL, Yoerger DR, Shank TM, Butterfield DA, Hayes JM, Schrenk MO, Olson EJ, Proskurowski G, Jakuba M, Bradley A, Larson B, Ludwig K, Glickson D, Buckman K, Bradley AS, Brazelton WJ, Roe K, Elend MJ, Delacour AJ, Bernasconi SM, Lilley MD, Baross JA, Summons RE and Sylva SP (2005) A serpentinite-hosted ecosystem: the Lost City hydrothermal field. *Science* **307**, 1428–1434.

King A, Schofield P, Howard K and Russell S (2015) Modal mineralogy of CI and CI-like chondrites by X-ray diffraction. *Geochimica et Cosmochimica Acta* **165**, 148–160.

Klein F, Bach W, Jöns N, McCollom T, Moskowitz B and Berquó T (2009) Iron partitioning and hydrogen generation during serpentinization of abyssal peridotites from 15°N on the Mid-Atlantic Ridge. *Geochimica et Cosmochimica Acta* **73**, 6868–6893.

Kostka JE and Nealson KH (1995) Dissolution and reduction of magnetite by bacteria. *Environmental Science & Technology* **29**, 2535–2540.

Kostka JE, Stucki JW, Nealson KH and Wu J (1996) Reduction of structural Fe(III) in smectite by a pure culture of *Shewanella putrefaciens* strain MR-1. *Clays and Clay Minerals* **44**, 522–529.

Liu D, Dong H, Bishop ME, Wang H, Agrawal A, Tritschler S, Eberl DD and Xie S (2011) Reduction of structural Fe(III) in nontronite by methanogen *Methanosarcina barkeri*. *Geochimica et Cosmochimica Acta* **75**, 1057–1071.

Marquart KA, Haller BR, Paper JM, Flynn TM, Boyanov MI, Shodunke G, Gura C, Jin Q and Kirk MF (2019) Influence of pH on the balance between methanogenesis and iron reduction. *Geobiology* **17**, 185–198.

McKay CP, Anbar AD, Porco C and Tsou P (2014) Follow the plume: the habitability of Enceladus. *Astrobiology* **14**, 352–355.

Pearce CI, Qafoku O, Liu J, Arenholz E, Heald SM, Kukkadapu RK, Gorski CA, Henderson CMB and Rosso KM (2012) Synthesis and properties of titanomagnetite ($Fe_3 - xTi_xO_4$) nanoparticles: a tunable solid-state Fe (II/III) redox system. *Journal of Colloid and Interface Science* **387**, 24–38.

Pignatelli I, Marrocchi Y, Vacher LG, Delon R and Gounelle M (2016) Multiple precursors of secondary mineralogical assemblages in CM chondrites. *Meteoritics & Planetary Science* **51**, 785–805.

Postberg F, Kempf S, Schmidt J, Brilliantov N, Beinsen A, Abel B, Buck U and Srama R (2009) Sodium salts in E-ring ice grains from an ocean below the surface of Enceladus. *Nature* **459**, 1098–1101.

Postberg F, Schmidt J, Hillier J, Kempf S and Srama R (2011) A salt-water reservoir as the source of a compositionally stratified plume on Enceladus. *Nature* **474**, 620–622.

Postberg F, Khawaja N, Abel B, Choblet G, Glein CR, Gudipati MS, Henderson BL, Hsu HW, Kempf S, Klenner F and Moragas-Klostermeyer G (2018a) Macromolecular organic compounds from the depths of Enceladus. *Nature* **558**, 564–568.

Postberg F, Clark RN, Hansen CJ, Coates AJ, Dalle Ore CM, Scipioni F, Hedman M and Waite J (2018b) Plume and surface composition of Enceladus. *Enceladus and the icy moons of Saturn* **5**, 129–162.

Postberg F, Sekine Y, Klenner F, Glein CR, Zou Z, Abel B, Furuya K, Hillier JK, Khawaja N, Kempf S, Noelle L, Saito T, Schmidt T, Shibuya T, Srama R and Tan S (2023) Detection of phosphates originating from Enceladus's ocean. *Nature* **618**, 489–493.

Postma D and Jakobsen R (1996) Redox zonation: equilibrium constraints on the Fe(III)/SO$_4$-reduction interface. *Geochimica et Cosmochimica Acta* **60**, 3169–3175.

Ray C, Glein CR, Waite JH, Teolis B, Hoehler T, Huber JA, Lunine J and Postberg F (2021) Oxidation processes diversify the metabolic menu on Enceladus. *Icarus* **364**, 114248.

Rosenberg ND, Browning L and Bourcier WL (2001) Modeling aqueous alteration of CM carbonaceous chondrites. *Meteoritics & Planetary Science* **36**, 239–244.

Russell MJ (2018) Green rust: the simple organizing 'seed' of all life?. *Life* **8**, 35.

Russell MJ, Hall AJ and Turner D (1989) In vitro growth of iron sulphide chimneys: possible culture chambers for origin-of-life experiments. *Terra Nova* **1**, 238–241.

Russell MJ, Daniel RM, Hall AJ and Sherringham JA (1994) A hydrothermally precipitated catalytic iron sulphide membrane as a first step toward life. *Journal of Molecular Evolution* **39**, 231–243.

Russell M, Hall A and Martin W (2010) Serpentinization as a source of energy at the origin of life. *Geobiology* **8**, 355–371.

Russell MJ, Barge LM, Bhartia R, Bocanegra D, Bracher PJ, Branscomb E, Kidd R, McGlynn S, Meier DH, Nitschke W, Shibuya T, Vance S, White L and Kanik I (2014) The drive to life on wet and icy worlds. *Astrobiology* **14**, 308–343.

Schwertmann U and Cornell R (2000) *Iron oxides in the laboratory: preparation and characterization*. 2nd Edn. Weinheim, Germany: Wiley-VCH Verlag GmbH.

Scott JJ, Breier JA, Luther III GW and Emerson D (2015) Microbial iron mats at the Mid-Atlantic ridge and evidence that Zetaproteobacteria may be restricted to iron-oxidizing marine systems. *PLoS ONE* **10**, e0119284.

Sekine Y, Shibuya T, Postberg F, Hsu H-W, Suzuki K, Masaki Y, Kuwatani T, Mori M, Hong PK, Yoshizaki M, Tachibana S and Sirono S (2015) High-temperature water–rock interactions and hydrothermal environments in the chondrite-like core of Enceladus. *Nature Communications* **6**, 1–8.

Sephton MA (2002) Organic compounds in carbonaceous meteorites. *Natural Product Reports* **19**, 292–311.

Stookey LL (1970) Ferrozine – a new spectrophotometric reagent for iron. *Analytical Chemistry* **42**, 779–781.

Taubner R-S, Pappenreiter P, Zwicker J, Smrzka D, Pruckner C, Kolar P, Bernacchi S, Seifert AH, Krajete A, Bach W, Peckmann J, Paulik C, Firneis M, Schleper C and Rittmann SKMR (2018) Biological methane production under putative Enceladus-like conditions. *Nature Communications* **9**, 1–11.

Tenelanda-Osorio LI, Parra JL, Cuartas-Restrepo P and Zuluaga JI (2021) Enceladus as a potential niche for methanogens and estimation of its biomass. *Life* **11**, 1182.

Thomas P, Tajeddine R, Tiscareno M, Burns J, Joseph J, Loredo T, Helfenstein P and Porco C (2016) Enceladus' measured physical libration requires a global subsurface ocean. *Icarus* **264**, 37–47.

Tomeoka K and Buseck PR (1985) Indicators of aqueous alteration in CM carbonaceous chondrites: microtextures of a layered mineral containing Fe, S, O and Ni. *Geochimica et Cosmochimica Acta* **49**, 2149–2163.

Trolard F, Duval S, Nitschke W, Ménez B, Pisapia C, Nacib JB, Andréani M and Bourrié G (2021) Mineralogy, geochemistry and occurrences of fougerite in a modern hydrothermal system and its implications for the origin of life. *Earth-Science Reviews* **255**, 103910.

Viollier E, Inglett P, Hunter K, Roychoudhury A and Van Cappellen P (2000) The ferrozine method revisited: Fe(II)/Fe(III) determination in natural waters. *Applied Geochemistry* **15**, 785–790.

Waite Jr JH, Combi MR, Ip WH, Cravens TE, Mcnutt Jr RL, Kasprzak W, Yelle R, Luhmann J, Niemann H, Gell D, Magee B, Fletcher G, Lunine J and Tseng W (2006) Cassini ion and neutral mass spectrometer: Enceladus plume composition and structure. *Science* **311**, 1419–1422.

Waite Jr JH, Lewis WS, Magee BA, Lunine JI, Mckinnon WB, Glein CR, Mousis O, Young DT, Brockwell T, Westlake J, Nguyen MJ, Teolis BD, Niemann HB, Mcnutt Jr, RL, Perry M and Ip WH (2009) Liquid water on Enceladus from observations of ammonia and 40Ar in the plume. *Nature* **460**, 487–490.

Waite JH, Glein CR, Perryman RS, Teolis BD, Magee BA, Miller G, Grimes J, Perry ME, Miller KE, Bouquet A, Lunine JI, Brockwell T and Bolton SJ (2017) Cassini finds molecular hydrogen in the Enceladus plume: evidence for hydrothermal processes. *Science* **356**, 155–159.

Weber KA, Achenbach LA and Coates JD (2006) Microorganisms pumping iron: anaerobic microbial iron oxidation and reduction. *Nature Reviews Microbiology* **4**, 752–764.

Zhang J, Dong H, Liu D, Fischer TB, Wang S and Huang L (2012) Microbial reduction of Fe(III) in illite–smectite minerals by methanogen *Methanosarcina mazei*. *Chemical Geology* **292**, 35–44.

Zolensky M, Barrett R and Browning L (1993) Mineralogy and composition of matrix and chondrule rims in carbonaceous chondrites. *Geochimica et Cosmochimica Acta* **57**, 3123–3148.

Zolotov MY (2007) An oceanic composition on early and today's Enceladus. *Geophysical Research Letters* **34**, 031234.